

Supplementary material for: “Scattering theory of thermal and bipolar thermoelectric diodes”

José Balduque^{1,2} and Rafael Sánchez^{1,2,3}

¹*Departamento de Física Teórica de la Materia Condensada, Universidad Autónoma de Madrid, 28049 Madrid, Spain*

²*Condensed Matter Physics Center (IFIMAC), Universidad Autónoma de Madrid, 28049 Madrid, Spain*

³*Instituto Nicolás Cabrera (INC), Universidad Autónoma de Madrid, 28049 Madrid, Spain*

(Dated: March 6, 2025)

In this supplementary material we give additional details useful for the discussion in the main text. Section, **S-I** presents the scattering matrices of the different regions of the conductor and how they lead to the global scattering matrix of the system. Section **S-II** gives a derivation of the analytical results demonstrating the rectification induced by a thermalization probe in a minimal model. The model including two resonant tunneling barriers separated by a thermalization probe is analyzed in Secs. **S-III** (linear response) and **S-IV**. The later includes a discussion of the physical mechanism leading to the bipolar thermoelectric diode, the effect of the coupling to the thermalization probe and the temperature dependence. The physical interpretation and temperature dependence of the screening-induced bipolar diode is given in Sec. **S-V**. Finally, we include in Sec. **S-VI** plots of the currents and rectification coefficients in different parameter configurations.

S-I. SCATTERING MATRICES

A. Matrix for the coupling to the probe

The coupling to the probe terminal is introduced by the scattering matrix [S1]:

$$\mathcal{S}^\lambda = \begin{pmatrix} 0 & \sqrt{1-\lambda} & 0 & i\sqrt{\lambda} \\ \sqrt{1-\lambda} & 0 & i\sqrt{\lambda} & 0 \\ i\sqrt{\lambda} & 0 & \sqrt{1-\lambda} & 0 \\ 0 & i\sqrt{\lambda} & 0 & \sqrt{1-\lambda} \end{pmatrix}, \quad (\text{S1})$$

where λ is the probability of an electron in region 2 to be absorbed and thermalized by the probe. In the matrix, indices 1 and 2 correspond to the conductor channels connecting to regions 1 and 3; indices 3 and 4 correspond to channels connected to the probe terminal. Note that λ is treated in the same footing as other transmission probabilities in the scattering region.

In the configuration considered in the main text, for $\lambda = 0$, transport between the other conductor terminals (L and R) is elastic. For $\lambda = 1$, all electrons are thermalized to the probe distribution when entering the central region. Transport can in that case be understood in terms of scattering between three thermal reservoirs (L, R and the probe) separated by regions 1 and 3.

B. Resonant tunneling barriers

In a mesoscopic conductor, resonant tunneling appears typically in double-barrier structures forming quantum dots or quantum wells. Considering symmetric barriers and a single resonant state, the single-channel scattering can be described by a Breit-Wigner [S2] scattering matrix

$$\mathcal{S}^{\text{RTB}} = \begin{pmatrix} 1 + \tau & \tau \\ \tau & 1 + \tau \end{pmatrix}, \quad (\text{S2})$$

with transmission amplitude

$$\tau = \frac{-i\Gamma}{E - \varepsilon + i\Gamma}, \quad (\text{S3})$$

where ε is the energy of the resonant state and Γ/\hbar is its inverse lifetime due to coupling to the modes outside the double barrier [S1].

C. Scattering matrix for the total system

When the transport is fully elastic in the system the total scattering matrix have to account for processes that involve both scattering regions \mathcal{S}_1 , \mathcal{S}_3 , and the possible coherent reflections between them, where electrons accumulate a kinetic phase $k(E)d$; with $k(E) = \sqrt{2m(E - U_2)}$ the electron wavenumber in region 2. This is done by taking into account that e.g., the right-outgoing wave from region 1 is the left-ingoing wave at region 3, multiplied by a phase factor $e^{ik(E)d}$, and solving for all the outgoing waves as functions of the ingoing ones [S3, S4]. Defining $E_\alpha = E - U_\alpha$, the total scattering matrix reads:

$$\begin{aligned} \mathcal{S}(E, \mathbf{U}) &= \begin{pmatrix} r(E, \mathbf{U}) & \tau(E, \mathbf{U}) \\ \tau(E, \mathbf{U}) & r'(E, \mathbf{U}) \end{pmatrix}, \\ \tau(E, \mathbf{U}) &= \frac{e^{ik(E)d}\Gamma^2}{e^{ik(E)d/l_0}E_1E_3 + (E_1 - i\Gamma)(E_3 - i\Gamma)} \\ r(E, \mathbf{U}) &= \frac{E_1(E_3 - i\Gamma) - e^{ik(E)d}E_3(E_1 - i\Gamma)}{e^{ik(E)d}E_1E_3 + (E_1 - i\Gamma)(E_3 - i\Gamma)} \\ r'(E, \mathbf{U}) &= \frac{E_3(E_1 - i\Gamma) - e^{ik(E)d}E_1(E_3 - i\Gamma)}{e^{ik(E)d}E_1E_3 + (E_1 - i\Gamma)(E_3 - i\Gamma)}. \end{aligned} \quad (\text{S4})$$

One should be careful when using the scattering matrix obtained by this approach to calculate injectivities for

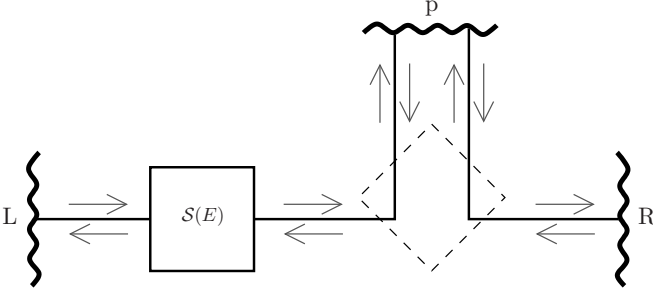


FIG. S1. Minimal configuration showing rectification by thermalization with a fully transparent coupling ($\lambda = 1$) to a probe terminal, p. A barrier represented by the scattering matrix S is placed between terminal L and the probe.

energies below \mathbf{U} , as it gives spurious divergences near the band bottom that are not present when using exact wave-function matching methods. This is relevant for the determination of the excess injected charge, as it involves the calculation of an integral starting from the energy origin. Here we have dealt numerically with this issue.

S-II. MINIMAL MODEL WITH THERMALIZATION

Consider the situation depicted in Fig. S1, with a fully transparently coupled ($\lambda = 1$) thermalization probe terminal, p, and a scattering region connecting it with terminal L with a transmission probability $\mathcal{T}(E) = |\mathcal{S}_{Lp}(E)|^2$. Electrons injected from terminal R are all absorbed by the probe. We impose $\mu_L = \mu_R = \mu$ to the conductor terminals and $I_p = J_p = 0$ to the probe.

The conductor currents are given by

$$I_L = \frac{2}{h} \int dE \mathcal{T}(E) (f_L - f_p) \quad (\text{S5})$$

$$I_R = \frac{2}{h} \int dE (f_R - f_p) = \frac{2}{h} (\mu - \mu_p), \quad (\text{S6})$$

for particles and

$$J_L = \frac{2}{h} \int dE (E - \mu) \mathcal{T}(E) (f_L - f_p) \quad (\text{S7})$$

$$J_R = \frac{2}{h} \int dE (E - \mu) (f_R - f_p) = \frac{\pi^2}{3h} (T_R^2 - T_p^2), \quad (\text{S8})$$

for heat. In the probe, $I_p = -I_L - I_R$ and $J_p = -J_L - J_R$. With charge and energy conservation, the current through the conductor is fully determined by the exact expressions for I_R and J_R above given by $\mu - \mu_p$ and $T_R^2 - T_p^2$. In order to have a diode effect, such that $I_L^F \neq I_L^B$ and $J_L^F \neq J_L^B$, it is hence enough to prove that $\mu_p^F \neq \mu_p^B$ and $T_p^F \neq T_p^B$, respectively.

For the thermoelectric case, it is easy to show that if \mathcal{T} is energy independent, so it induces no thermoelectric effect in the probe, we get $I_L = 2\mathcal{T}(\mu - \mu_p)/h$

independently of the temperature T_L . Therefore, the only current-conserving solution is $\mu_p = \mu$, indeed giving $I^F = I^B = 0$. If we now consider an energy-dependent transmission probability,

$$I_L^F = \frac{2}{h} \int dE \mathcal{T}(E) [f(T + \Delta T) - f_p] \quad (\text{S9})$$

and

$$I_L^B = \frac{2}{h} \int dE \mathcal{T}(E) [f(T) - f_p] \quad (\text{S10})$$

are necessarily different, as long as the scatterer breaks electron-hole symmetry i.e., if it has a finite thermoelectric response. In that case, from Eq. (S6) we get $\mu_p^F \neq \mu_p^B$.

For the heat currents, it is sufficient to assume that $0 < \mathcal{T} < 1$. In the simplest case where it is energy independent, we get

$$J_L^F = \frac{\mathcal{T}\pi^2}{3h} [(T + \Delta T)^2 - (T_p^F)^2] = \frac{\pi^2}{3h} [T^2 - (T_p^F)^2]$$

$$J_L^B = \frac{\mathcal{T}\pi^2}{3h} [T^2 - (T_p^B)^2] = \frac{\pi^2}{3h} [(T + \Delta T)^2 - (T_p^B)^2]. \quad (\text{S11})$$

Solving for the probe temperatures, we get:

$$(T_p^F)^2 = (\mathcal{T} - 1)T^2 + \mathcal{T}(\Delta T^2 + 2T\Delta T) \quad (\text{S12})$$

$$(T_p^B)^2 = (\mathcal{T} - 1)T^2 - \mathcal{T}(\Delta T^2 + 2T\Delta T), \quad (\text{S13})$$

clearly showing a diode effect, $T_p^F \neq T_p^B$.

S-III. LINEAR RESPONSE OF A THERMALIZATION PROBE

Consider two scattering regions, $\alpha = 1, 3$ separated by a transparently coupled probe terminal, such that all electrons injected from terminals L and R are either reflected at the barriers or absorbed by the probe. The electrochemical potential, μ_p , and temperature, T_p , of the probe need to be calculated to fulfill the conditions $I_p = J_p = 0$. Current is only due to a temperature difference ΔT applied to terminal L in the forward (F), or to R in the backward configuration (B). Let us consider first the forward case, where we expand the particle and heat currents as:

$$I_L^F = -G_1 \Delta \mu_p^F + L_1 (\Delta T - \Delta T_p^F) \quad (\text{S14})$$

$$I_R^F = -G_3 \Delta \mu_p^F - L_3 \Delta T_p^F \quad (\text{S15})$$

$$J_L^F = -M_1 \Delta \mu_p^F + K_1 (\Delta T - \Delta T_p^F) \quad (\text{S16})$$

$$J_R^F = -M_3 \Delta \mu_p^F - K_3 \Delta T_p^F, \quad (\text{S17})$$

where $\Delta \mu_p^F = \mu_p^F - \mu$ and $\Delta T_p^F = T_p^F - T$. G_α , L_α , M_α and K_α are the electrical conductance, Seebeck coefficient, Peltier coefficient and thermal conductance of

scattering region α , respectively. Solving for the probe conditions, we get:

$$\begin{aligned}\Delta\mu_p^F &= \frac{L_1K_3 - L_3K_1}{G_\Sigma K_\Sigma - L_\Sigma M_\Sigma} \Delta T \\ \Delta T_p^F &= \frac{G_\Sigma K_1 - L_1M_\Sigma}{G_\Sigma K_\Sigma - L_\Sigma M_\Sigma} \Delta T,\end{aligned}\quad (\text{S18})$$

where the subindex Σ indicates the sum over L and R. With these, we get the currents:

$$\begin{aligned}I_L^F &= \frac{G_1L_3K_1 + G_3L_1K_3 - L_1L_3M_\Sigma}{G_\Sigma K_\Sigma - L_\Sigma M_\Sigma} \Delta T \\ J_L^F &= \frac{K_1K_3G_\Sigma - K_1L_3M_3 - K_3L_1M_1}{G_\Sigma K_\Sigma - L_\Sigma M_\Sigma} \Delta T.\end{aligned}\quad (\text{S19})$$

For the backward currents, we simply replace $1 \leftrightarrow 3$ in Eqs. (S18) and (S19). This way we obtain

$$\Delta\mu_p^F = -\Delta\mu^B, \quad (\text{S20})$$

as well as $I_L^F = -I_L^B$ and $J_L^F = -J_L^B$. As expected, there is no rectification in the linear regime.

A. Antisymmetric configuration

A particularly interesting case is when the transmission of region 3, $\mathcal{T}_3(E)$ is the reflection of $\mathcal{T}_1(E)$ over the electrochemical potential. Then, $G_1 = G_3$, $L_1 = -L_3$, $M_1 = -M_3$ and $K_1 = K_3$. In that case, we get:

$$\Delta\mu_p^F = \frac{L_1}{2G_1} \Delta T \quad \text{and} \quad \Delta T_p^F = \frac{\Delta T}{2}, \quad (\text{S21})$$

and

$$I_L^F = 0 \quad \text{and} \quad J_L^F = \frac{K}{2} \Delta T. \quad (\text{S22})$$

In the same way, $I_L^B = 0$. Therefore in this case only the nonlinear contributions are responsible for the thermoelectric particle currents.

S-IV. BIPOLAR DIODE BY THERMALIZATION

The thermalization-induced bipolar thermoelectric diode occurs around the condition when the resonances of scatterers 1 and 3 are antisymmetric with respect to the base electrochemical potential, μ , and have a similar (but opposite) response to electrochemical and temperature differences with the probe terminal. That is the case represented in Fig. S2. In order to understand this effect, it is important to first notice that the temperature difference is the only thermodynamic force. Hence, the flow of heat is well defined by the second law of thermodynamics (and by everyone's intuition) and goes from the hot to the cold reservoir, i.e., it has opposite sign in the forward and the backward configurations. Differently, the sign of

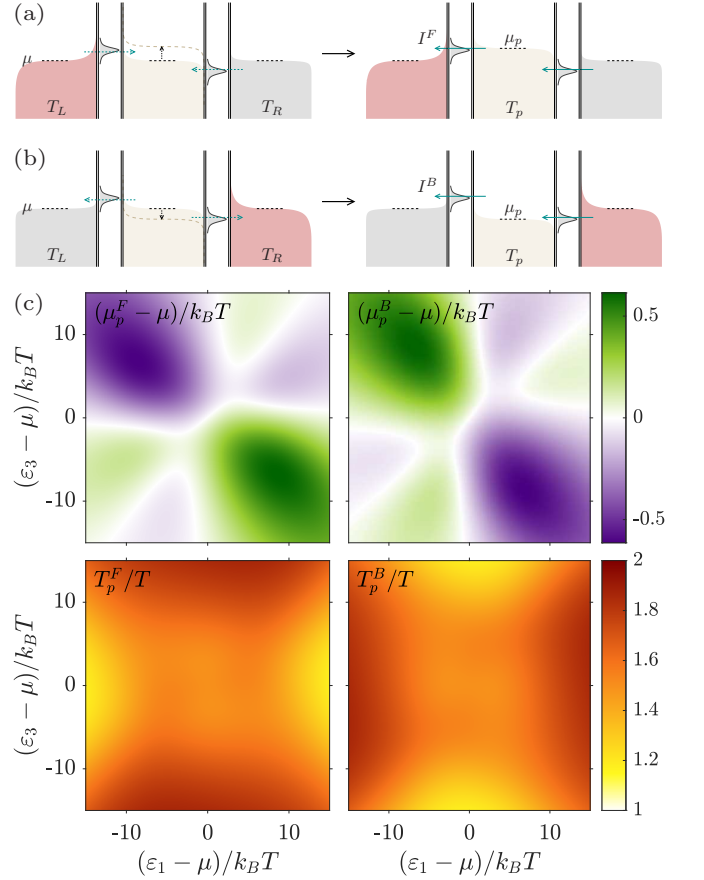


FIG. S2. Mechanism for bipolar rectification induced by the thermalization probe. The two panels show how the contributions to the particle flows through the two barriers change with the chemical potential developed at the probe in (a) the forward and (b) the backward configurations. The left column shows the sign of the (purely) thermoelectric contributions when $\mu_p = \mu$. In the right column, these contributions have modified μ_p , resulting in the reversal of the flows through one of the barriers. (c) Electrochemical potential and temperature developed at the thermalization probe in the forward and backward configurations. Parameters: $\Gamma = 3k_B T$, $\mu = 40k_B T$, and $\Delta T/T = 1$.

the thermoelectric current is not fixed by any thermodynamic law. In this particular case, it depends on the developed potential in the probe.

Consider first the forward configuration, cf. Fig. S2(a), in which the thermalization probe initially has an electrochemical potential μ but its temperature is already the one fixed by the probe conditions $I_p = J_p = 0$. Clearly, $T_R < T_p < T_L$, see Fig. S2(c). For concreteness, we fix $\varepsilon_1 = -\varepsilon_3 > \mu$. In such a situation, the thermoelectric response of the two resonant tunneling barriers results in charge flowing into the conductor: particles flow from the hotter to the colder reservoir when the resonance is over the electrochemical potential, and in the opposite direction when it is below [S5]. The probe terminal hence increases its electrochemical potential, as shown in

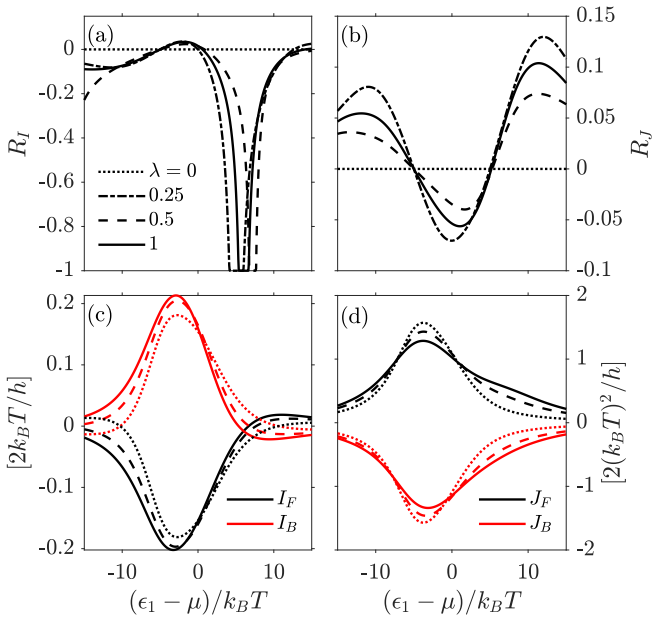


FIG. S3. Effect of the coupling to the thermalization probe on (a) the thermoelectric and (b) thermal rectification coefficients. (c) and (d) show the corresponding particle and heat currents. Parameters: $\Gamma = 3k_B T$, $\mu = 40k_B T$, $\Delta T = T$, $d = 2h/\sqrt{8mk_B T}$ and $(\epsilon_3 - \mu) = -5k_B T$.

Fig. S2(c). The voltage established between terminals L and R and the probe introduces another contribution to the particle current (additional to the temperature-driven thermoelectric response). In this particular configuration, the distance $\epsilon_1 - \mu_p$ is reduced, while $\epsilon_3 - \mu_p$ increases, so transport through barrier 1 is most sensitive to this change. Eventually (when $\mu_p - \mu$ attains the thermovoltage of barrier 1 under a temperature difference $T_L - T_p$), the voltage-induced contribution developed by thermalization is able to reverse the flow of particles through barrier 1. The particle current through the conductor then flows from R to L and $I^F < 0$.

In the backward configuration, see Fig. S2(b), the same arguments apply, with the difference that, as the resonances are opposite, when exchanging the temperatures T_L and T_R , the initial thermoelectric contributions have the opposite sign, i.e., the flow into the L and R terminals. Then, the electrochemical potential of the probe tends to diminish, see Fig. S2(c), again approaching the resonance coupled to the hot reservoir (ϵ_3), so it is the contribution through barrier 3 the one that is finally reversed. As a consequence, we again have particles flowing from R to L, i.e., $I^B < 0$.

In the perfectly antisymmetric case, we furthermore have $I^F = I^B < 0$.

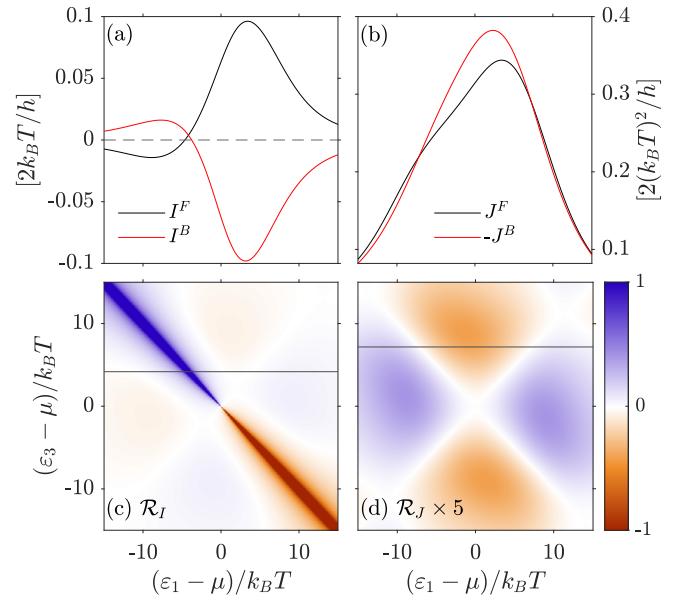


FIG. S4. Thermalization diode. Forward and backward (a) particle and (b) heat currents as functions of ϵ_1 tuned along $(\epsilon_3 - \mu)/k_B T = 4.8$ and 8.7 , respectively, indicated by black lines in (c) and (d), correspondingly. The later panels show the thermoelectric and heat rectification coefficients, as functions of both resonances. The thermalization probe is fully coupled ($\lambda = 1$), and $\mu \gg U_\alpha$, so the band bottom has no effect. Parameters: $\Gamma = 3k_B T$, $\mu = 40k_B T$, and $\Delta T/T = 1/2$.

A. Effect of the finite coupling to the probe

In the main text we have discussed the case where all the electrons entering the center region are thermalized by the probe, with $\lambda = 1$. The effect of a finite coupling to the probe is plotted in Fig. S3, showing that the rectification coefficients and currents have the same qualitative behaviour. In particular, the bipolar thermoelectric effect is robust to finite λ , though the region where it appears is reduced with the opacity of the coupling.

B. Temperature dependence

We plot in Fig. S4 the currents and rectification coefficient for $\Delta T = T/2$, showing that, though expectedly weaker, the same effects discussed in the main text for $\Delta T = T$ also appear in this case. Antireciprocal thermoelectric currents are restricted to a narrower region around $\epsilon_1 = -\epsilon_3$. This is because the shift of μ_2 is not large enough to invert one of the currents far from the antisymmetric condition.

Figure S5 shows the temperature dependence of the thermalization-induced bipolar thermoelectric and thermal diode effects for two configurations of Fig. 3 of the main text. The one for the thermoelectric case is chosen slightly de-tuned from the antisymmetric configuration with $\epsilon_1 + \epsilon_3 = 0$, for which we find $\mathcal{R}_I = 1$ for ev-

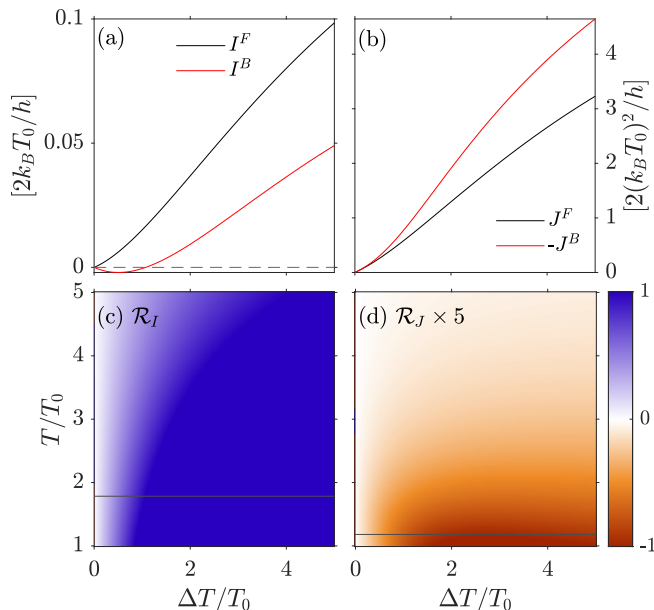


FIG. S5. Temperature dependence of the thermalization-induced rectification. Forward and backward (a) particle and (b) heat currents as functions of ΔT for temperatures $T = 1.8T_0$ and $1.2T_0$, respectively, indicated by black lines in (c) and (d), correspondingly. The later panels show the thermoelectric and heat rectification coefficients, as functions of $\Delta T/T_0$ and T/T_0 , for configurations of Fig. 3 of the main text with $(\epsilon_1 - \mu)/k_B T_0 = -6$ and 0 , and $(\epsilon_1 - \mu)/k_B T_0 = 7$ and 10 respectively. The remaining parameters are the same, with $\lambda = 1$.

ery ΔT , T . In this particular configuration, the bipolar thermoelectric diode still occurs for almost all temperature configurations, see Figs. S5(a) and S5(c). Only close to the linear response regime, with small temperature differences, we have $\mathcal{R}_I < 1$. As shown in Figs. S5(b) and S5(d), the difference of the forward and backward currents increases with ΔT , as expected. The thermal rectification coefficient however saturates. We have introduced a new reference temperature T_0 specifically for this plot.

S-V. BIPOLAR DIODE BY SCREENING EFFECTS

The screening-induced bipolar thermoelectric diode occurs when the transmission energy dependence presents two nonzero contributions, one above and one below the reference electrochemical potential, as sketched in Fig. S6 and plotted in Fig. S7(a): a wide double-peak at positive energies, due to the two Breit-Wigner resonances being close in energy, and a sharp peak at negative energies, due to the Fabry-Perot interference in region 2. The nonlinear response will depend on how the internal energies U_α react to the temperature increase in one of the reservoirs, therefore modifying the overall trans-

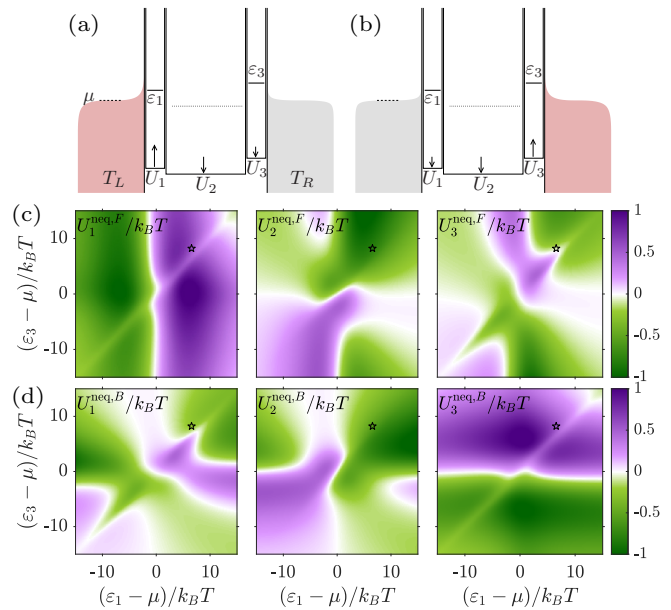


FIG. S6. Scheme of the developed internal potentials, U_α , induced by charge accumulation in (a) the forward and (b) the backward configurations. Solid lines mark the energy of the resonances, $\epsilon_1 < \epsilon_3$, with the dotted line indicating the position of a Fabry-Perot interference peak. Under the appropriate conditions, this effect results in a bipolar thermoelectric diode with particles flowing from L to R in both configurations. Developed nonequilibrium electrostatic energies in the three regions for the (c) forward and (d) backward configurations. Same configuration as in Fig. 3 in the main text, with $\lambda = 0$, $d = 2h/\sqrt{8mk_B T}$, $\Gamma = 1k_B T$, $\mu = 40k_B T$ and $\Delta T = T$.

mission probability, $\mathcal{T}(\{\mathbf{U}\})$. The internal energies are obtained self-consistently by solving the change in the induced charge, δq_α , in each region. This is given by the injectivities $\nu_{l\alpha}$ from terminal j into region α via

$$\frac{\delta q_\alpha}{-e} = \int dE \sum_j [\nu_{j\alpha}(E, \mathbf{U}) f_j(E) - \nu_{j\alpha}^{\text{eq}} f_{\text{eq}}(E)], \quad (\text{S23})$$

see main text. Clearly for a given region the injectivity is larger for the terminal with which it is directly coupled i.e., $\nu_{L1} \gg \nu_{R1}$ and $\nu_{R3} \gg \nu_{L3}$, see Figs. S7(b) and S7(c). Hence, one expects the potential of region 1(3) to change more in the forward (backward) configuration. The opposite region in each configuration is expected to be barely affected by the temperature increase, therefore this small modification can then also be influenced by the charging of the other regions via the self-consistency.

To get a better intuition, let us focus on a particular configuration, as the one sketched in Fig. S6, with both Breit-Wigner resonances having energies over the chemical potential, $\mu < \epsilon_1 < \epsilon_3$. Close to equilibrium (for small temperature differences), the current is dominated by the Breit-Wigner resonances, so particles flow from L to R in the forward, and opposite in the backward configuration. Consider first the forward configuration,

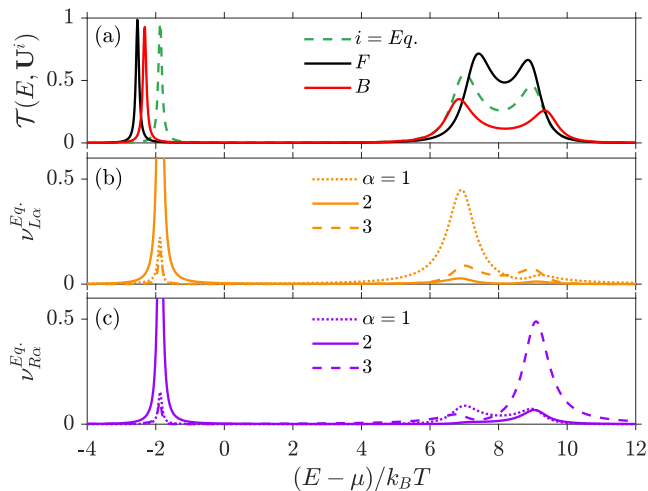


FIG. S7. (a) Transmission probability when the system is in equilibrium (solid green), and in the forward (dashed black) and backward (dotted red) configurations, once the electrostatic potentials have build-up in the three areas as a result of the corresponding non-equilibrium situation. (b)-(c) In-junctivities in regions $\alpha = 1, 2, 3$ from reservoirs L and R , respectively. The parameters correspond to the ones where $I^B = I^F \neq 0$ in Fig. 3(e) of the main text, marked by \star in Fig. 3(a) [as well in Fig. S6(c) and S6(d)].

depicted in Fig. S6(a). The change in the nonequilibrium electrostatic energies is shown in Fig. S6(c) as the resonances are tuned. The temperature increase in terminal L contributes to charge region 1 by increasing the occupation of the lead at the energies around ε_1 (for enhancing the tail of the Fermi distribution). Hence, U_1 is expected to increase. The next region to consider is region 2, whose coupling to terminal L is weaker. This region features a sharp interference peak below the chemical potential, thus resulting on a decrease of the charge with respect to the equilibrium state (states of the lead below the chemical potential are less occupied when increasing the terminal temperature), so U_2 decreases. Finally, region 3 is in this case little affected by the temperature variation in terminal L, but it can be indirectly affected by the potential variation in the regions in between: the change in U_1 and U_2 also affects region 3 and compete in the resulting U_3 in a complicated manner. In this particular case, it also decreases. With this, the two Breit-Wigner resonances in regions 1 and 3 are then brought closer in energy, resulting in a narrower and sharper feature at positive energies in the transmission probability, see Fig. S7(a), which is favorable for the thermoelectric current from L to R.

The same arguments apply to the backward configuration, depicted in Fig. S6(b). The developed U_α^{neq} are shown in Fig. S6(d). In this case, it results in U_1 decreasing and U_3 increasing, which separates the two Breit-Wigner resonances and makes the double peak at positive energies wider and lower, see Fig. S7(a). Thus the thermoelectric contribution at positive energies (from

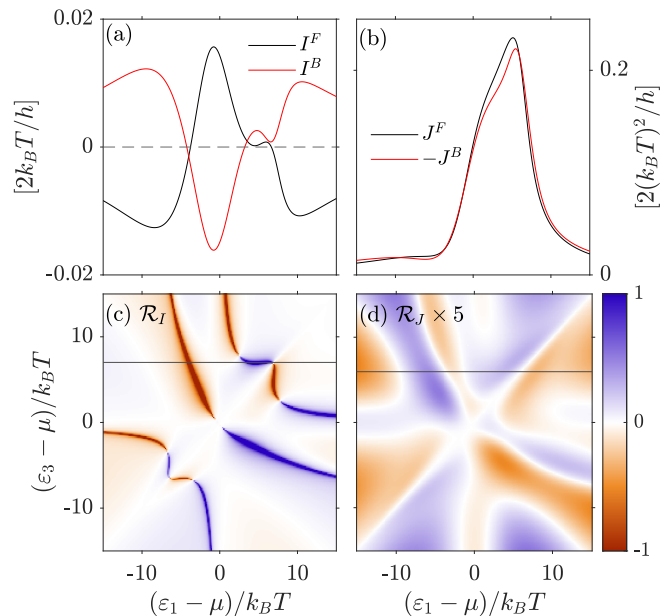


FIG. S8. Rectification by screening. Forward and backward (a) particle and (b) heat currents as functions of ε_1 , for fixed $(\varepsilon_3 - \mu)/k_B T = 8.2$ and 7.5 as marked by black lines in (c) and (d), respectively. The later show the dependence of \mathcal{R}_I and \mathcal{R}_J with gating the RTBs. Parameters: $\lambda=0$, $d = 2h/\sqrt{8mk_B T}$, $\Gamma = k_B T$, $\mu = 40k_B T$, $\Delta T/T = 1/2$.

the hot R to the cold L) is reduced. The Fabry-Perot interference peak, being at negative energies contributes to transport in the opposite direction (from L to R). Eventually, the Breit-Wigner contribution gets so weak that the Fabry-Perot contribution, which is robust to the change in temperature, starts to dominate. At that point, the current through the system changes sign, so particles flow from L to R, as in the forward configuration.

In other words, the antireciprocal effect is due to a change of the contribution of positive- and negative-energy spectral features, which contribute oppositely to the thermoelectric response.

A. Temperature dependence

Figure S8 shows the thermoelectric and thermal rectification properties at a lower temperature difference than the one considered in the main text, $\Delta T = T/2$. The same features observed in Fig. 3 of the main text appear, with smaller rectification coefficients, as expected. The bipolar thermoelectric diode occurs in narrower regions of the gate-voltage map.

The temperature dependence is plotted in Fig. S9 for the particular gating corresponding to Fig. S7 (marked with a \star in Fig. 3(a) of the main text). It shows that the bipolar thermoelectric diode occurs for wide temperature ranges, cf. Figs. S9(a) and S9(c), showing a threshold at low temperatures and temperature gradients which is

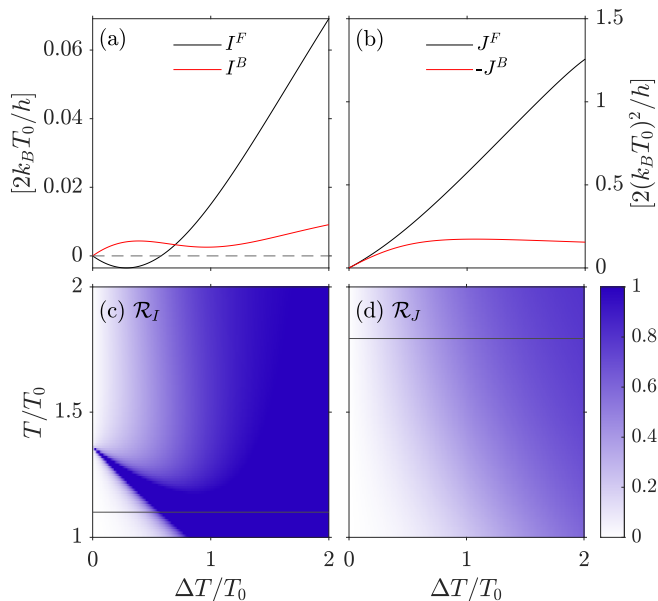


FIG. S9. Temperature dependence of the screening induced rectification. Forward and backward (a) particle and (b) heat currents as functions of ΔT for temperatures $T = 1.1T_0$ and $1.8T_0$, respectively, indicated by black lines in (c) and (d), correspondingly. The later panels show the thermoelectric and heat rectification coefficients, as functions of $\Delta T/T_0$ and T/T_0 . The remaining parameters correspond to the ones where $I_B = I_F \neq 0$ in Fig. 3(e) of the main text, marked by \star in Fig. 3(a) [as well in Fig. S6(c) and S6(d)].

tunable with gating. The thermal currents show a robust diode effect, with the I^F increasing with ΔT , while I^B saturates and even shows negative thermal differential conductance for large enough ΔT , cf. Fig. S9(b). The thermal rectification coefficient increases both with T and ΔT , see Fig. S9(d).

S-VI. CHARGE AND HEAT CURRENTS

Figures S10, S11, S12 and S13 show the forward and backward particle and heat currents as well as the thermoelectric and thermal rectification coefficients for the different configurations as functions of the quantum dot linewidth, Γ , and of the distance between barriers 1 and 3, d (for the thermalization free case with $\lambda = 0$, Fig. S12). The thermoelectric currents reach values of the order of nA at $T = 1$ K and $\Delta T/T = 1$, where a bidimensional GaAs device would have a carrier concentration of $\sim 10^{12} \text{ cm}^{-2}$ and sizes of tens of nm for the explored regimes.

[S1] M. Büttiker, Coherent and sequential tunneling in series barriers, *IBM J. Res. Dev.* **32**, 63 (1988).
[S2] G. Breit and E. Wigner, Capture of slow neutrons, *Phys. Rev.* **49**, 519 (1936).
[S3] S. Datta, *Electronic Transport in Mesoscopic Systems* (Cambridge University Press, 1995).

[S4] R. Sánchez, C. Gorini, and G. Fleury, Extrinsic thermoelectric response of coherent conductors, *Phys. Rev. B* **104**, 115430 (2021).
[S5] G. Benenti, G. Casati, K. Saito, and R. S. Whitney, Fundamental aspects of steady-state conversion of heat to work at the nanoscale, *Phys. Rep.* **694**, 1 (2017).

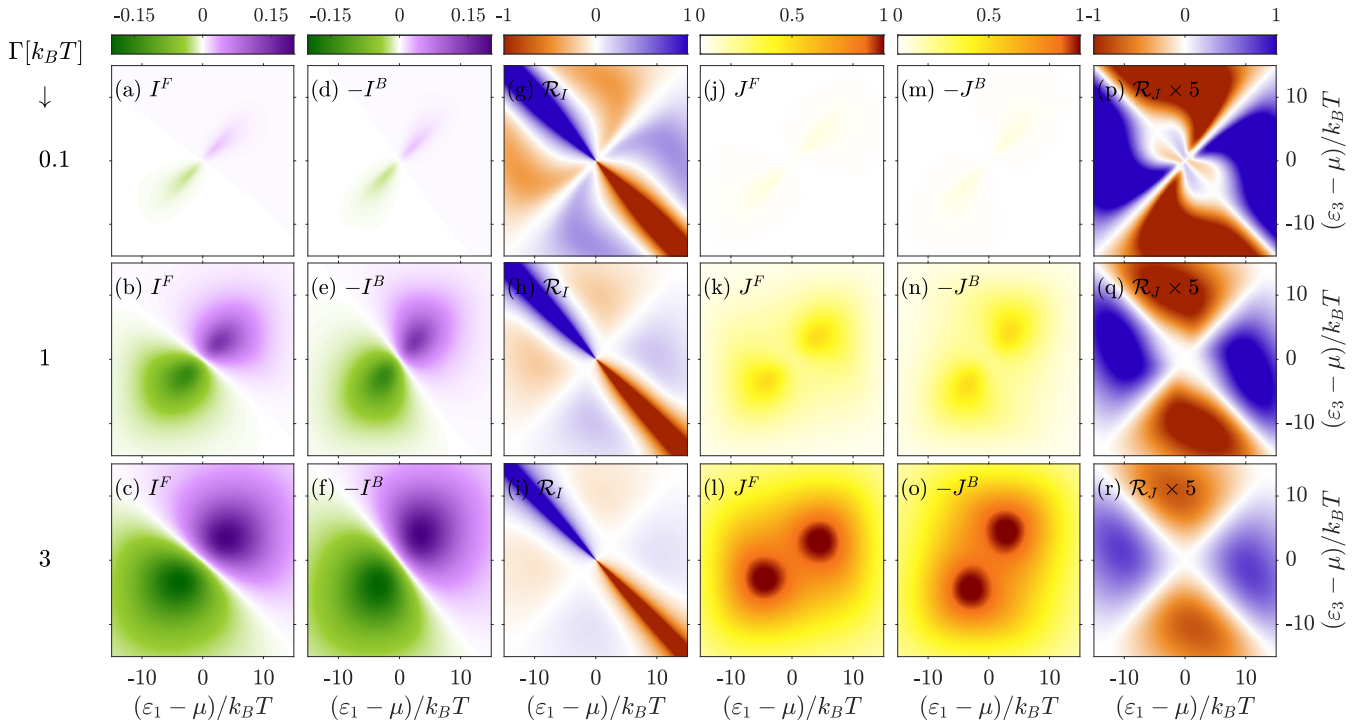


FIG. S10. (a)-(c) Forward and (d)-(f) backward particle currents, and (g)-(i) thermoelectric rectification for the double resonant tunneling barrier conductor sandwiching a strong thermalization region ($\lambda = 1$) and neglecting screening, as functions of the resonance energies, ε_1 and ε_3 and for increasing quantum dot linewidth, Γ . (j)-(l), (m)-(o) and (p)-(r) show the corresponding the heat quantities. In all cases, $\Delta T = T$.

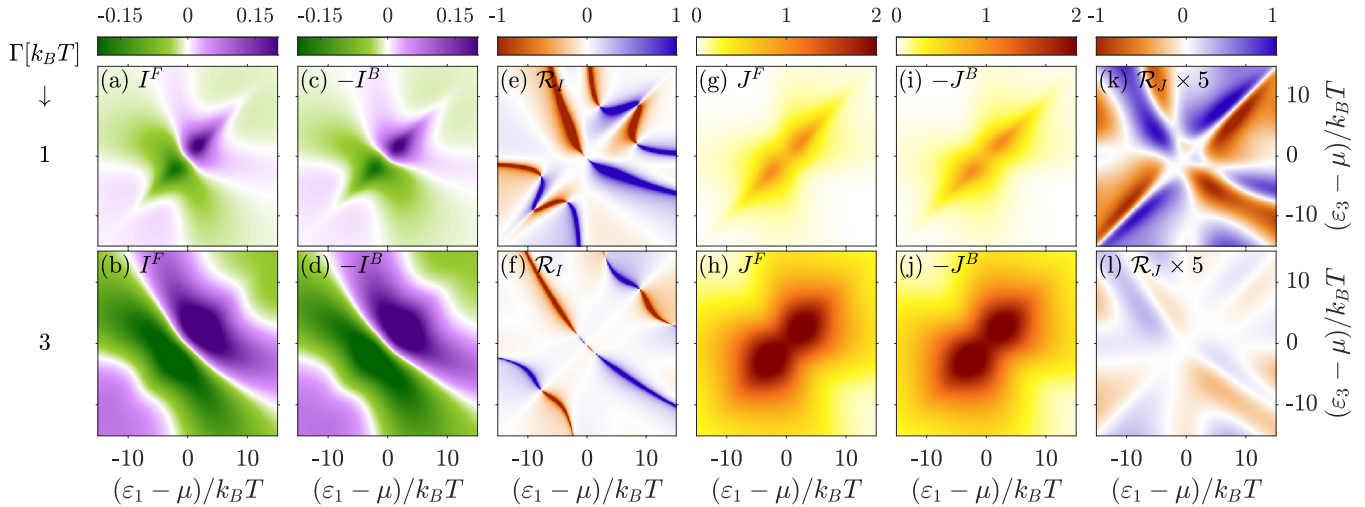


FIG. S11. Same as Fig. S10 in the elastic case with $\lambda = 0$ including screening effects, for $d = 2\hbar/\sqrt{8mk_B T}$ and $\mu = 40k_B T$.

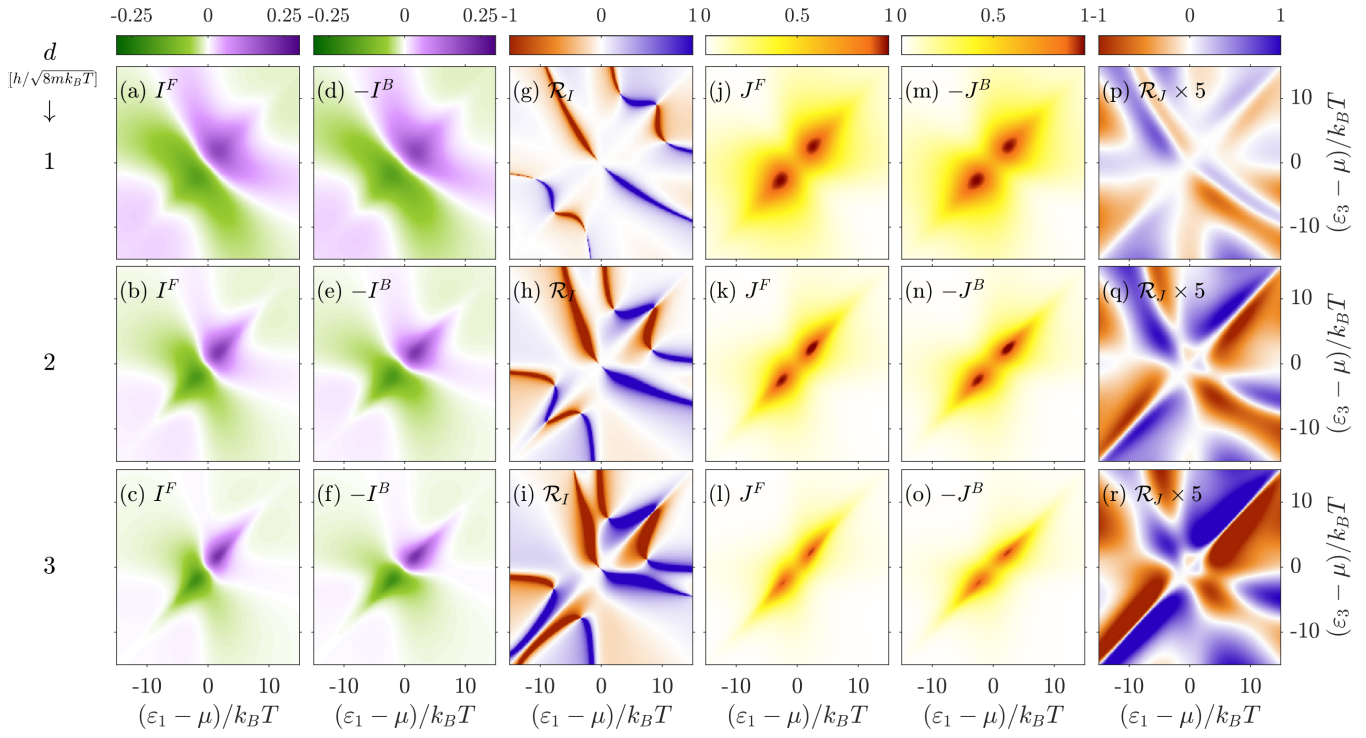


FIG. S12. Same as Fig. S11 for $\Gamma = k_B T$ and for different lengths of region 2, d , which controls the position and width of the Fabry-Perot resonance at energies below the chemical potential.

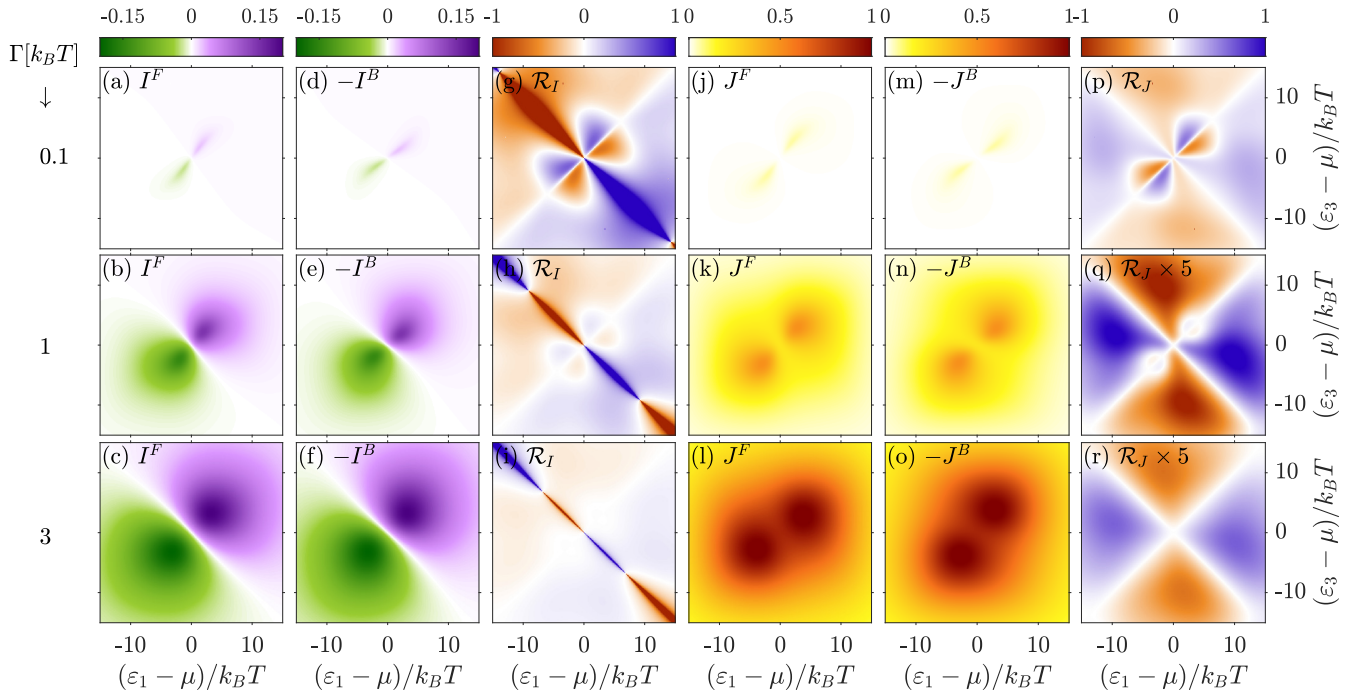


FIG. S13. Same as Fig. S11 in the strong thermalization regime with $\lambda = 1$.